Thin Solid Films 553 (2014) 58–62

Contents lists available at ScienceDirect

Thin Solid Films

journal homepage: www.elsevier.com/locate/tsf

Local structure relaxation in nanocrystalline $Ni_{1-x}O$ thin films

A. Anspoks *, A. Kalinko, R. Kalendarev, A. Kuzmin

Institute of Solid State Physics, University of Latvia, 8 Kengaraga Street, LV-1063 Riga, Latvia

ARTICLE INFO

Available online 20 September 2013

Keywords:
Nickel oxide
Thin films
EXAFS spectroscopy
Molecular dynamics

ABSTRACT

Non-stoichiometric nickel oxide ($Ni_{1-x}O$) thin films were prepared by DC magnetron sputtering technique in mixed Ar/O_2 atmosphere and studied by synchrotron radiation Ni K-edge x-ray absorption spectroscopy, x-ray diffraction and scanning electron microscopy. The use of advanced modelling technique, combining classical molecular dynamics with ab initio multiple-scattering extended x-ray absorption fine structure calculations, allowed us to describe the structure relaxation and dynamics in nanocrystallites and to estimate their size and the concentration of nickel vacancies.

1. Introduction

Nickel oxide (NiO) thin films are technologically an important material, which finds a broad range of practical applications including but not limited to transparent oxide electronics [1], resistive memories [2], electrochromic devices [3], gas sensors [4], giant magnetoresistive spin valve structures [5], catalysis [6] and rechargeable batteries [7]. A performance of all these devices depends largely on the thin film's crystallinity, texture and stoichiometry.

Bulk NiO has a cubic rock-salt crystal structure (Fm-3 m) undergoing a weak cubic-to-rhombohedral distortion (R-3 m) below the Néel temperature $T_N = 523$ K due to the magnetostriction effect [8]. It is a p-type semiconductor, having usually an oxygen excess due to the presence of nickel vacancies (V_{Ni}) [9–11]. Upon size reduction down to nanoscale, the influence of crystallite surface increases leading to the atomic structure relaxation. An expansion of lattice volume has been found in nanosized NiO by diffraction [12–15] (Fig. 1) and x-ray absorption spectroscopy [16–19]. It was tentatively explained in [12,15] by a negative pressure due to the repulsive interaction of the parallel surface defect dipoles at small particle sizes. The unit cell volume in nanoparticles becomes equal to that in crystalline nickel oxide for crystallite size above about 20 ± 5 nm, taking into account the accuracy of the lattice constant determination in [12–15].

Lattice volume expansion upon size reduction is rather common for nanooxides, but is opposite to that in metal nanoparticles, where shrinkage of the lattice is usually observed (see, for example, in [20]). The origin of structural relaxation in nanooxides is debatable and is often related to surface effect, stoichiometry, metal oxidation state and the presence of impurities. Recently, we have shown that the presence of nickel vacancies is required for the explanation of the nearest Ni – O distance shortening in nanosize NiO, which simultaneously shows Ni – Ni distance expansion [21]. Therefore, the knowledge of local atomic structure is crucial for the understanding of structure relaxation phenomena in NiO thin film.

The local atomic structure of nanomaterials can be probed by extended x-ray absorption fine structure (EXAFS) spectroscopy [22,23]. Recent achievements [24] in the EXAFS data analysis methodology based on a complex modelling approach using molecular dynamics (MD) simulations allowed us to study local atomic structure and lattice dynamics in crystalline NiO [18,19], $SrTiO_3$ [25], ReO_3 [26], Ge [27] and $LaCoO_3$ [28] as well as in nanocrystalline NiO [21,29]. In the MD–EXAFS method, the configuration-averaged EXAFS spectrum is generated using the full power of modern ab initio multiple-scattering theory [30] from a set of atomic configurations, obtained during the MD run. As a result, the method requires a small number of model parameters, which are used in the force-field potential to describe interactions between atoms in a material.

In this study we applied the MD–EXAFS method [21,24], combining ab initio EXAFS calculations with classical molecular dynamics, to investigate the atomic structure relaxation and the role of nickel vacancies in nanocrystalline $Ni_{1-x}O$ thin films.

2. Experimental details

Non-stoichiometric nanocrystalline $Ni_{1-x}O$ thin films were produced using reactive dc-magnetron sputtering of metallic nickel target and were deposited on three substrates (silicon, glass and polyimide tape). The film deposition was performed at three Ar/O_2 ratios equal to 0/100 (TF1), 50/50 (TF2) and 90/10 (TF3). Thus obtained thin films had thicknesses of about 1 μm and dark brown colour, suggesting the presence of nickel vacancies [9–11]. Commercial microcrystalline NiO powder (c-NiO, Aldrich, 99%), having green colour, was used for comparison.

The crystallinity and morphology of the films were characterized by x-ray diffraction (XRD) (PANalytical, Model X'Pert Pro MPD) and scanning electron microscopy (SEM) (Carl Zeiss, Model EVO 50 XVP), respectively.

* Corresponding author. Tel.: +371 67251691; fax: +371 67132778.
E-mail address: andris.anspoks@cfi.lu.lv (A. Anspoks).

0040-6090/$ – see front matter © 2013 Elsevier B.V. All rights reserved.
http://dx.doi.org/10.1016/j.tsf.2013.08.132

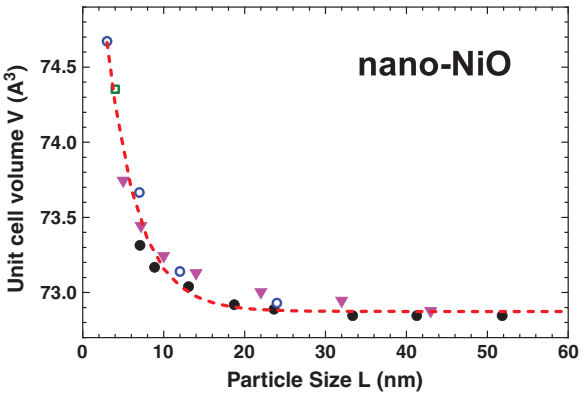

Fig. 1. Dependence of the unit cell volume on the nanoparticle size (data taken from XRD studies, solid circles from [12], empty circles from [13], empty box from [14], solid triangles from [15]). Dashed line corresponds to the fitted formula $V = V_0 + A \exp(-L / B)$, where V is the unit cell volume (in Å^3), L is the particle size (in nm), $V_0 = 72.874$ Å^3, $A = 3.9419$ Å^3, and $B = 3.8009$ nm.

XRD patterns of the films deposited on polyimide tape are shown in Fig. 2. The film TF1 shows preferential orientation in (100) direction, the film TF2 in (100) and (110) directions, and the film TF3 in (111) and (110) directions. The size of the crystallites, according to the Scherrer method, is between 6 nm (TF3) and 18 nm (TF1), suggesting that the crystallinity of the films is influenced by the sputtering atmosphere, i.e. Ar/O_2 ratio.

SEM images of $Ni_{1-x}O$ thin films, simultaneously deposited on silicon, glass and polyimide film with the gas ratio $Ar/O_2 = 90/10$, reveal that their morphology strongly depends on substrate material. Films deposited on polyimide tape have the smoothest surface, but those deposited on silicon have the coarsest surface (Fig. 3).

The Ni K-edge x-ray absorption spectra were measured in transmission mode at the HASYLAB/DESY C (CEMO) bending magnet beamline [31]. The storage ring DORIS III operated at E = 4.44 GeV and I_{max} = 140 mA. The x-ray radiation was monochromatized by a 40% detuned Si(111) double-crystal monochromator, and the beam intensity was monitored using two ionization chambers filled with argon and krypton gases. A liquid He flow cryostat was used to perform temperature dependent measurements in the range between 6 and 300 K. The samples were optimized by making a stack of thin films, simultaneously sputtered on polyimide tape, in order to achieve the absorption Ni K-edge jump value $\Delta\mu \approx 1$. The EXAFS oscillations $\chi(k)$ were extracted and analyzed following the conventional procedure [32] using the EDA software package [33].

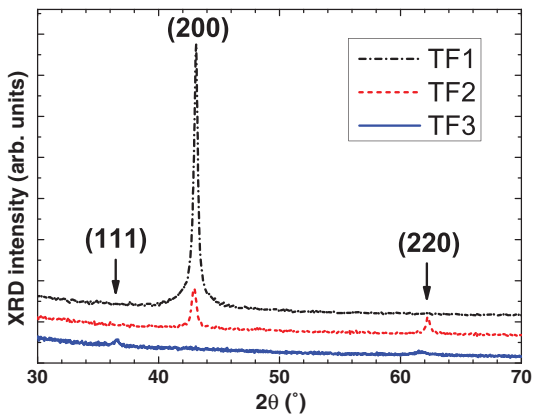

Fig. 2. XRD patterns of $Ni_{1-x}O$ thin films prepared at three Ar/O_2 gas ratios equal to 0/100 (TF1), 50/50 (TF2) and 90/10 (TF3).

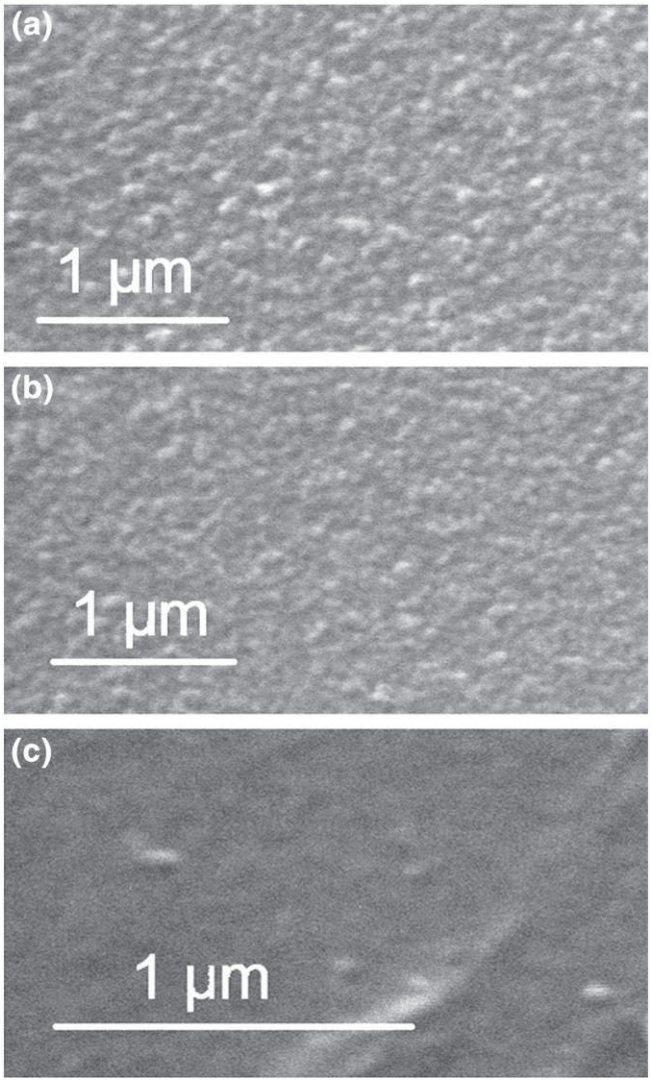

Fig. 3. SEM images of $Ni_{1-x}O$ thin films simultaneously sputtered on (a) silicon, (b) glass and (c) polyimide film with $Ar/O_2 = 90/10$. Operating voltage was 25 kV.

3. Results and discussion

3.1. Extended x-ray absorption fine structure (EXAFS)

Experimental Ni K-edge EXAFS spectra $\chi(k)k^2$ and their Fourier transforms (FTs) measured at T = 300 K for thin films, c-NiO and nanoparticles (data are taken from [21]) are shown in Fig. 4. Note the high quality of the obtained EXAFS data in a wide k-space ranging up to 17 Å^{-1} for all samples. The structural peaks in FT are well visible up to 10 Å in microcrystalline c-NiO. The main difference between the EXAFS spectra of c-NiO and thin films manifests in the signal behaviour at large wave number values: it is significantly damped in the films. Also the amplitude of peaks in the FTs of EXAFS for the films becomes significantly reduced upon increasing distance. Such behaviour is typical for nanocrystalline materials: it is caused by an increase of the amount of under-coordinated atoms at the crystallite surface upon a reduction of crystallite size and by induced static disorder due to structure relaxation. As one can see in Fig. 5, the EXAFS spectra of thin films show pronounced temperature dependence, suggesting that the thermal disorder effect is important along with the static one.

A contribution into the total EXAFS spectrum from the first two coordination shells (the peaks at ~1.7 Å and ~2.7 Å in Fig. 4) can be analyzed in the single-scattering approximation [18,19]. Therefore, it was isolated by the Fourier filtering procedure in the R-space range of

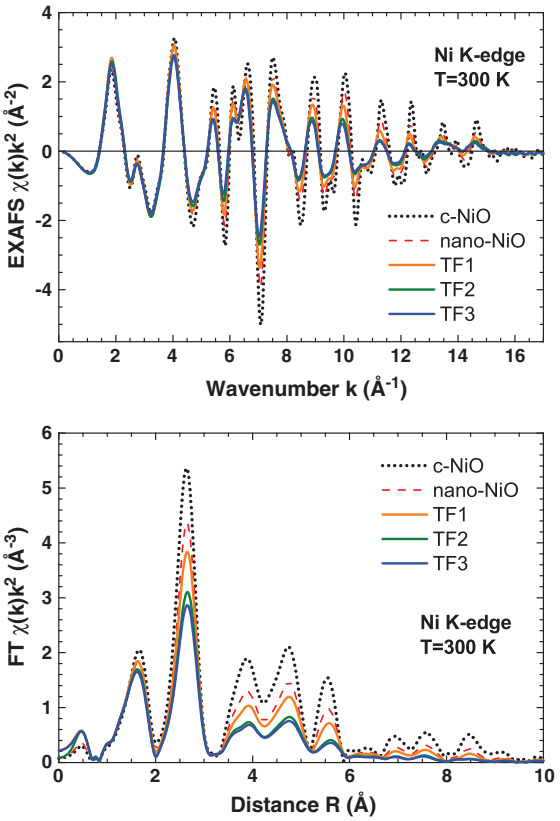

Fig. 4. Experimental Ni K-edge EXAFS spectra $\chi(k)k^2$ and their Fourier transforms for the thin film samples compared with microcrystalline c-NiO and NiO nanoparticles (data taken from [18]). All data measured at T = 300 K.

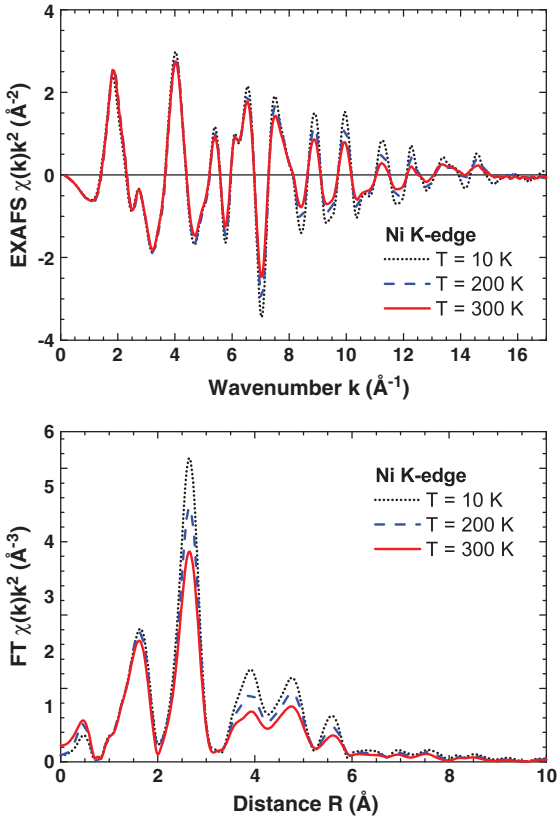

Fig. 5. Experimental Ni K-edge EXAFS spectra $\chi(k)k^2$ and their Fourier transforms for the thin film TF3 (Ar/O_2 = 90/10) at three selected temperatures. Note the EXAFS oscillations damping at high-k values due to thermal disorder.

0.7–3.2 Å and best fitted in the k-space range of 2–17 $Å^{-1}$ using the two-component Gaussian model [32]. The scattering amplitude and phase shift functions for the Ni–O_1 and Ni–Ni_2 atom pairs, used in the fits, were extracted from the low temperature (T = 6 K) experimental data for c-NiO sample, assuming the crystallographic value of the lattice parameter a_0 = 4.176 Å [34]. The obtained values of coordination numbers (N), interatomic distances (R) and mean-square relative displacements (MSRDs) (σ^2) at T = 300 K are given in Table 1. To break the correlation between MSRD and coordination number N we have used the following procedure. For each sample the MSRD values were first determined at lowest temperature (T = 10 K) as a function of N from the fit of two EXAFS signals $\chi(k)k^2$ and $\chi(k)k^3$. The crossing point of these two dependences gave us the final value of N, which was kept constant in the fitting procedure at all other temperatures.

As one can see in Table 1, the values of the average interatomic distances R(Ni–Ni_2) in the second coordination shell of Ni in all nanosized samples are larger than those in microcrystalline c-NiO. This result confirms the unit cell volume expansion upon a decrease of the NiO nanocrystallite size, observed previously by XRD studies [12–15]. The largest unit cell volume (V = 74.27 $Å^3$) is found for the film TF3, thus indicating that this sample has the smallest crystallite size. The unit cell volume decreases in the film TF2 (V = 74.11 $Å^3$) and further in the film TF1 (V = 74.00 $Å^3$).

The temperature dependences of the MSRDs σ^2 are shown in Fig. 6. Note that the determined MSRD values are relative to the low temperature c-NiO data, i.e. $\Delta\sigma^2 = \sigma^2(T) - \sigma^2$(c-NiO, T = 6 K). MSRDs for the films contain both temperature dependent (thermal) and constant (static) parts. The temperature dependences of MSRDs suggest that a contribution of the thermal disorder in the films and nano-NiO is close to that in the bulk NiO (c-NiO). However, the static disorder in the films is larger than in nano-NiO powder: it increases upon a decrease of the crystallite size but remains constant upon temperature variation. These results correlate well with temperature dependent XRD studies of nanosized (~4 nm) NiO [14]. It was found that in the temperature range of up to 300 K the difference between lattice constants of nanosized and bulk NiO powders remains nearly constant, and the lattice thermal expansion is close [14].

Upon a decrease of crystallite size, nickel atoms located at the surface become under-coordinated and, thus, contribute into a decrease of the average coordination numbers. In Fig. 7 we show the dependence of the average coordination number N_{Ni2} in the second shell of nickel on the cubic nanoparticle size (L = la_0). For large crystallites, it approaches the value of 12 nickel atoms, corresponding to that in the bulk NiO. Taking into account the values of N_{Ni2} reported in Table 1, one can conclude that the size of crystallites in the films is about 4–6 unit cells (or about 1.7–2.5 nm). Note that one should be very careful when using coordination numbers for any conclusions, because they are subject to systematic errors and other factors, including the presence of vacancies and

Table 1
The structural parameters (N, R, $\Delta\sigma^2$) for the first (O1) and second (Ni2) coordination shells of nickel at T = 300 K obtained by conventional approach based on the single-scattering approximation. Data for NiO nanoparticles from [21] are provided for comparison. a_0 is the lattice parameter ($a_0 = 2^{1/2} R_{Ni2}$), and V is the unit cell volume ($V = a_0^3$).

	c-NiO	Nano-NiO	TF1 (Ar/O_2 = 0/100)	TF2 (Ar/O_2 = 50/50)	TF3 (Ar/O_2 = 90/10)
N_{O1}	6.0	6.0	6.0	6.0	6.0
R_{O1} (Å)	2.089	2.082	2.085	2.080	2.085
$\Delta\sigma^2_{O1}$ ($Å^2$)	0.0016	0.0028	0.0044	0.0054	0.0061
N_{Ni2}	12.0	11.1	9.9	9.6	9.2
R_{Ni2} (Å)	2.954	2.962	2.969	2.970	2.972
$\Delta\sigma^2_{Ni2}$ ($Å^2$)	0.0027	0.0035	0.0046	0.0059	0.0064
a_0 (Å)	4.178	4.189	4.198	4.200	4.203
V ($Å^3$)	72.92	73.53	74.00	74.11	74.27

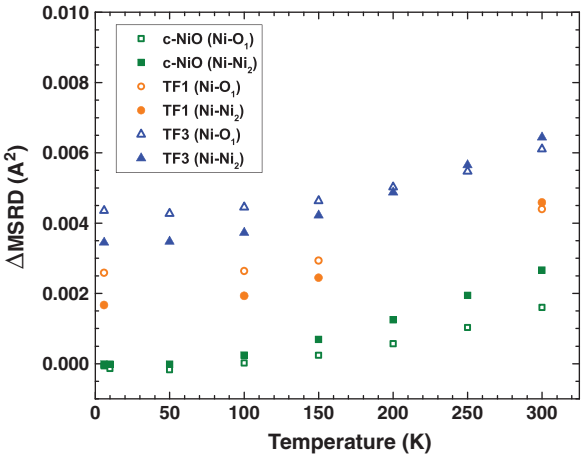

Fig. 6. Temperature dependence of the relative mean-square relative displacements (ΔMSRD) $\Delta\sigma^2$ for the first (Ni–O_1) and second (Ni–Ni_2) coordination shells in c-NiO and $Ni_{1-x}O$ thin films relative to the MSRD value in c-NiO at T = 6 K.

particle shape. However, they give good estimate and feeling about the observed trend, which is in line with the results from XRD.

While the lattice expansion in nanosized NiO correlates well with an increase of the second shell R(Ni–Ni_2) distance, the average distance R(Ni–O_1) in the first coordination shell shows opposite behaviour, i.e. it contracts (Table 1). Such behaviour is not possible in the perfect cubic lattice, however in real nanoparticles/nanocrystallites the effect is caused by the Ni – O bond shortening at the surface and around nickel vacancies [19,35,36], which are present in our dark brown thin films [9–11]. In the next section we will demonstrate how the average size of nanoparticles/nanocrystallites and the concentration of nickel vacancies can be simultaneously estimated by taking into account multiple-scattering effects in the EXAFS analysis.

3.2. MD–EXAFS modelling

In order to better understand the controversial structure relaxation in $Ni_{1-x}O$ thin films we used the recently developed modelling method MD–EXAFS [21,24], combining ab initio EXAFS calculations with classical molecular dynamics (MD). This approach goes beyond the single-scattering approximation used in the conventional analysis and utilizes full power of the ab initio multiple-scattering theory [30]. Classical MD simulations in the canonical (NVT) ensemble at T = 300 K were performed by the DL_POLY 4.02 code [37] using the force-field potential,

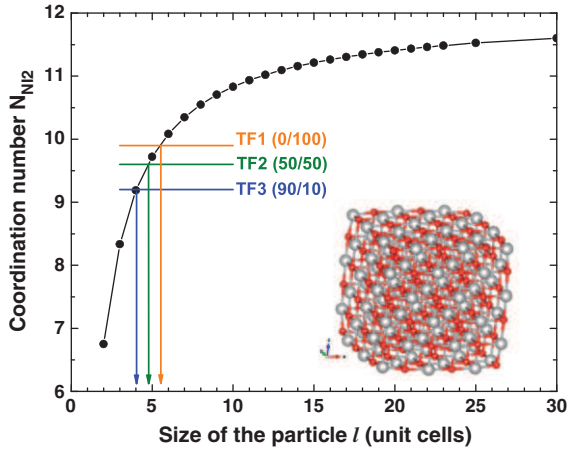

Fig. 7. Dependence of the average coordination number N_{Ni2} in the second shell of nickel on the cubic nanoparticle size (L = la_0). The parameters for three $Ni_{1-x}O$ thin films are indicated. The inset shows the relaxed nanoparticle model with l = 3 (3 × 3 × 3 unit cells).

described in details in [21]. The EXAFS spectra for each instantaneous atomic configuration were calculated by the ab initio real-space multiple-scattering FEFF8 code [38]. Finally, the configuration-averaged EXAFS spectra were compared with the experimental ones to validate the model.

NiO nanocrystallites were modelled as cubic-shaped nanoparticles having different sizes and different numbers of evenly distributed nickel vacancies. Nickel vacancy concentration (C_{vac}) is defined as: $C_{vac} = N_{vac} / N_O$, where N_{vac} is the number of nickel vacancies and N_O is the number of oxygen atoms. As it has been shown previously [21], the presence of nickel vacancies causes strong local structure relaxation around them: the nearest oxygen atoms around the Ni vacancy move away towards nickel atoms by ~0.2 Å, but the nearest nickel atoms move towards the vacancy by ~0.08 Å. The relaxation of the next neighbours around the vacancy is insignificant.

Our MD–EXAFS simulation procedure consists of two steps. In the first step, we used the MD method to calculate a series of atomic configuration snapshots, from which the average distances (R_{O1} and R_{Ni2}) in the first two coordination shells of Ni atoms were extracted and compared to that obtained from the single-scattering EXAFS analysis (Table 1). The agreement between two sets of distances within the desired accuracy (±0.005 Å) was used as a criterion to adjust the force-field parameters employed in the MD simulations. This step allowed us to narrow the range of possible solutions and to reduce significantly the total computational time by minimizing the amount of resource demanding EXAFS spectra calculations. As a result, after the first simulation step we have filtered out a small set of the model nanoparticles having different sizes and different concentration of nickel vacancies but giving desired values of the average R_{O1} and R_{Ni2} distances.

In the second step, a direct comparison between the experimental and configuration-averaged EXAFS spectra was performed, and the residual between two spectra was minimized by adjusting the force-field parameters. The configuration-averaged EXAFS spectra were calculated for each model nanoparticle after performing the MD run and taking into account all multiple-scattering contributions up to the seventh order. In this way, the influence of particle size, structure relaxation, thermal disorder and the presence of nickel vacancies were incorporated into the model. Moreover, the large region (up to 6.5 Å) in R-space probed by EXAFS, which includes eight coordination shells and many multiple-scattering contributions [19,21], allowed us to select the final one from a set of possible solutions, obtained after the first step.

The experimental and model EXAFS spectra are compared in Fig. 8 for the case of the film TF3 (Ar/O_2 = 90/10), showing good agreement in both k and R space. Similar agreement was found for other two (TF1 and TF2) thin films. The size of the model nanoparticles and the concentration of nickel vacancies for all thin film samples are reported in Table 2. As one can see, these results correlate well with those of the analysis for the first two shells by conventional EXAFS method, suggesting that the average size of the nanocrystallites decreases in the series: TF1 (Ar/O_2 = 0/100), TF2 (Ar/O_2 = 50/50), and TF3 (Ar/O_2 = 90/10). Note that the Ni vacancy concentration increases with a decrease of the nanocrystallite size.

The obtained size of nanocrystallites is in good agreement with that estimated from the coordination number (N_{Ni2}) in the second shell of nickel (Fig. 7). This is an expected result, because small number of vacancies does not affect the coordination number significantly. It is more interesting to compare the difference between average size of nanocrystallites obtained by XRD (using Scherrer method) and EXAFS (from coordination number (N_{Ni2}) and MD–EXAFS methods). The two experimental techniques show qualitatively similar trends, however Scherrer method gives systematically larger values for nanocrystallite size: from 6 nm in the film TF3 to 18 nm in the film TF1. This fact can be explained by the presence of particles of various sizes. The Bragg peaks in the XRD patterns are significantly broadened upon decreasing crystallite size and, thus, become masked by the noise for crystallites with a size smaller than ~2 nm. Therefore, the XRD signal is dominated

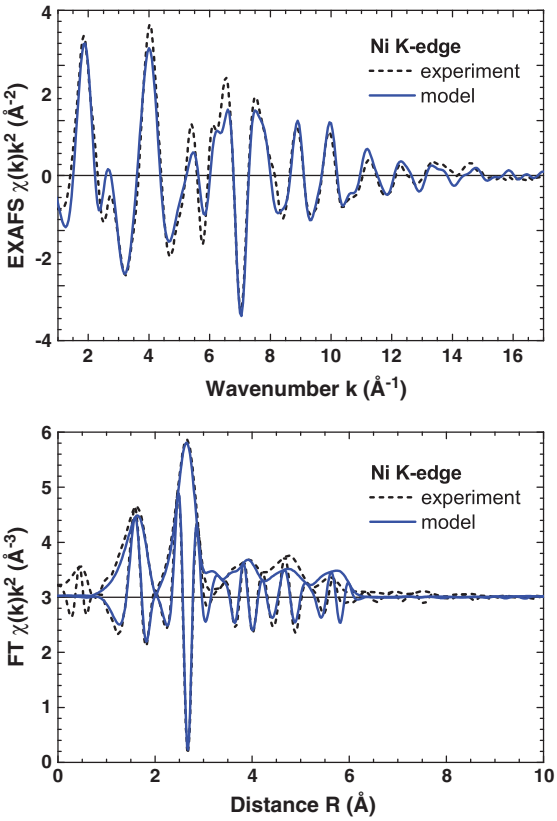

Fig. 8. Experimental (dashed line) and model (solid line) Ni K-edge EXAFS spectra $\chi(k)k^2$ and their Fourier transforms for the film TF3 ($Ar/O_2 = 90/10$) at T = 300 K.

by the contribution coming from the largest crystallites present in the sample. On the contrary, EXAFS feels all absorbing nickel atoms, regardless the state and size of the matter, so it is averaging over the size distribution.

4. Conclusions

Non-stoichiometric nickel oxide ($Ni_{1-x}O$) thin films, prepared by DC magnetron sputtering technique in mixed Ar/O_2 atmosphere, were studied by synchrotron radiation Ni K-edge x-ray absorption spectroscopy, x-ray diffraction and scanning electron microscopy.

It was found that the morphology of the films depends on the substrate type (silicon, glass, polyimide tape) and sputtering conditions (Ar/O_2 ratio). The smallest surface roughness was observed on polyimide tape, while the smallest crystallite size was obtained upon sputtering at low oxygen content ($Ar/O_2 = 90/10$). All films have cubic rock-salt crystal structure (Fm-3 m) with texture, which depends on sputtering conditions. Films with larger crystallites have preferable crystallite orientation (100), but upon decreasing the size of the crystallites it changes to (110) and (111).

The atomic structure in nanocrystalline $Ni_{1-x}O$ thin films experiences strong relaxation and lattice expansion upon a decrease of the nanocrystallite size. At the same time, the average $Ni-O_1$ bond length in the first coordination shell of nickel atoms contracts due to structure relaxation at the surface (especially, at corners and edges of the crystallites) and near the nickel vacancies. This phenomenon cannot be revealed by XRD, and shows the particular value of the x-ray absorption spectroscopy.

The thermal contributions to the MSRD in the first and second coordination shells of nickel in the films are close to that in the bulk nickel oxide that suggests a similarity of their lattice dynamics. This conclusion is confirmed also by the thermal expansion data for NiO nanocrystallites, obtained by XRD [14]. However, upon a decrease of the crystallite size the static contribution to the MSRD increases due to structure relaxation, caused by the lattice expansion and the presence of nickel vacancies.

Table 2
The size of the model nanoparticles, which give the best agreement with the experimental EXAFS spectra measured at T = 300 K. $L = la_0$ is the size of the nanoparticle (l is the number of unit cells, a_0 is the lattice parameter), and C_{vac} is the concentration of nickel vacancies.

	Nano-NiO	TF1 ($Ar/O_2 = 0/100$)	TF2 ($Ar/O_2 = 50/50$)	TF3 ($Ar/O_2 = 90/10$)
l (unit cells)	9	6	5	4
L (nm)	3.6	2.3	1.9	1.5
C_{vac} (%)	0.4	1.0	1.4	1.6

Acknowledgements

The authors are grateful to Dr. R. Chernikov for assistance during EXAFS measurements at DESY, Dr. A. Mishnov for assistance during XRD measurements and K. Kundzins for help with SEM experiments. This work was supported by the Latvian Science Council Grant No. 187/2012 and European Social Fund within the project 2009/0138/1DP/1.1.2.1.2/09/IPIA/VIAA/004 ("Support for Doctoral Studies at University of Latvia"). The EXAFS experiments at HASYLAB/DESY have been supported by the European Community's Seventh Framework Programme under grant agreement no. 226716 (Project I-20100110 EC).

References

[1] H. Ohta, M. Hirano, K. Nakahara, H. Maruta, T. Tanabe, M. Kamiya, T. Kamiya, H. Hosono, Appl. Phys. Lett. 83 (2003) 1029.
[2] S. Seo, M.J. Lee, D.H. Seo, E.J. Jeoung, D.S. Suh, Y.S. Joung, I.K. Yoo, I.R. Hwang, S.H. Kim, I.S. Byun, J.-S. Kim, J.S. Choi, B.H. Park, Appl. Phys. Lett. 85 (2004) 5655.
[3] G.A. Niklasson, C.G. Granqvist, J. Mater. Chem. 17 (2007) 127.
[4] M. Ando, J. Zehetner, T. Kobayashi, M. Haruta, Sensors Actuators B 36 (2003) 513.
[5] E.Y. Tsymbal, D.G. Pettifor, Solid State Phys. 56 (2001) 113.
[6] X.-Y. Peng, W. Li, X.-X. Liu, P.-J. Hua, J. Appl. Polym. Sci. 105 (2007) 2260.
[7] Q. Pan, J. Liu, J. Solid State Electrochem. 13 (2009) 1591.
[8] W.L. Roth, Phys. Rev. 110 (1958) 1333.
[9] H. Sato, T. Minami, S. Takata, T. Yamada, Thin Solid Films 236 (1993) 27.
[10] O. Kohmoto, H. Nakagawa, Y. Isagawa, A. Chayahara, J. Magn. Magn. Mater. 226 (2001) 1629.
[11] J. Yu, K.M. Rosso, S.M. Bruemmer, J. Phys. Chem. C 116 (2012) 1948.
[12] L. Li, L. Chen, R. Qihe, G. Li, Appl. Phys. Lett. 89 (2006) 134102.
[13] M. Ghosh, K. Biswas, A. Sundaresan, C.N.R. Rao, J. Mater. Chem. 16 (2006) 106.
[14] X.G. Zheng, H. Kubozono, H. Yamada, K. Kato, Y. Ishiwata, C.N. Xu, Nat. Nanotechnol. 3 (2008) 724.
[15] S.A. Makhlouf, M.A. Kassem, M.A. Abdel-Rahim, J. Mater. Sci. 44 (2009) 3438.
[16] A. Kuzmin, J. Purans, A. Rodionov, J. Phys. Condens. Matter 9 (1997) 6979.
[17] E. Avendaño, A. Kuzmin, J. Purans, A. Azens, G.A. Niklasson, C.G. Granqvist, Phys. Scr. T115 (2005) 464.
[18] A. Anspoks, A. Kuzmin, A. Kalinko, J. Timoshenko, Solid State Commun. 150 (2010) 2270.
[19] A. Anspoks, A. Kuzmin, J. Non-Cryst. Solids 357 (2011) 2604.
[20] R. Lamber, S. Wetjen, N.I. Jaeger, Phys. Rev. B 51 (1995) 10968.
[21] A. Anspoks, A. Kalinko, R. Kalendarev, A. Kuzmin, Phys. Rev. B 86 (2012) 174114.
[22] H. Modrow, Appl. Spectrosc. Rev. 39 (2004) 183.
[23] A.I. Frenkel, A. Yevick, C. Cooper, R. Vasic, Annu. Rev. Anal. Chem. 4 (2011) 23.
[24] A. Kuzmin, R.A. Evarestov, J. Phys. Condens. Matter 21 (2009) 055401.
[25] A. Kuzmin, R.A. Evarestov, J. Phys. Conf. Ser. 190 (2009) 012024.
[26] A. Kalinko, R.A. Evarestov, A. Kuzmin, J. Purans, J. Phys. Conf. Ser. 190 (2009) 012080.
[27] J. Timoshenko, A. Kuzmin, J. Purans, Cent. Eur. J. Phys. 9 (2011) 710.
[28] A. Kuzmin, V. Efimov, E. Efimova, V. Sikolenko, S. Pascarelli, I.O. Troyanchuk, Solid State Ionics 188 (2011) 21.
[29] A. Anspoks, A. Kalinko, R. Kalendarev, A. Kuzmin, J. Phys. Conf. Ser. 430 (2013) 012027.
[30] J.J. Rehr, R.C. Albers, Rev. Mod. Phys. 72 (2000) 621.
[31] K. Rickers, W. Drube, H. Schulte-Schrepping, E. Welter, U. Brüggmann, M. Herrmann, J. Heuer, H. Schulz-Ritter, Am. Inst. Phys. Conf. Proc. 882 (2007) 905.
[32] V.L. Aksenov, M.V. Kovalchuk, A.Yu. Kuzmin, Yu. Purans, S.I. Tyutyunnikov, Crystallogr. Rep. 51 (2006) 908.
[33] A. Kuzmin, Physica B 208–209 (1995) 175.
[34] D. Rodic, V. Spasojevic, V. Kusigerski, R. Tellgren, H. Rundlof, Phys. Status Solidi B 218 (2000) 527.
[35] A.M. Ferrari, C. Pisani, J. Chem. Phys. 127 (2007) 174711.
[36] S. Park, H.-S. Ahn, C.-K. Lee, H. Kim, H. Jin, H.-S. Lee, S. Seo, J. Yu, S. Han, Phys. Rev. B 77 (2008) 134103.
[37] I.T. Todorov, W. Smith, K. Trachenko, M.T. Dove, J. Mater. Chem. 16 (2006) 1611.
[38] A.L. Ankudinov, B. Ravel, J.J. Rehr, S.D. Conradson, Phys. Rev. B 58 (1998) 7565.